Dielectronic satellite spectrum of heliumlike vanadium

P. Beiersdorfer, M. H. Chen, R. E. Marrs, M. B. Schneider, and R. S. Walling
High Temperature Physics Division, University of California, Lawrence Livermore National Laboratory, Livermore, California 94550

(Received 12 November 1990; revised manuscript received 1 March 1991)

K x-ray spectra of heliumlike vanadium and associated dielectronic satellite emission from lithiumlike, berylliumlike, and boronlike vanadium have been observed with a high-resolution crystal spectrometer from the Lawrence Livermore electron-beam ion trap. Measurements include dielectronic satellite spectra from the *KLL*, *KLM*, *KLN*, *KLO*, and *KLP* resonance. Many transitions are identified that are unresolved in plasma observations, and transition energies are measured with high accuracy. Comparisons of calculated and observed intensities of selected transitions show few differences.

I. INTRODUCTION

X-ray emission produced by dielectronic recombination of heliumlike ions plays a major role in the diagnostics of plasmas. In low-density plasmas such as those found in the sun and tokamaks, the intensity of dielectronic satellite lines in low-Z and medium-Z heliumlike ions is commonly measured to determine the plasma electron temperature or to ascertain the existence of non-Maxwellian electron-energy distributions [1–7]. Spectra of the dielectronic satellites have been observed from low-density plasmas for most elements up to nickel [8,9].

In this paper we describe high-resolution measurements of the $1s2l^m nl'$ ($m=1,2,3$; $n=2,3,4,5,6$) dielectronic satellite spectrum of heliumlike V^{21+} from an electron-beam ion trap (EBIT). EBIT is a novel tool for atomic-physics studies that employs an electron beam to ionize, trap, and excite ions of a particular element [10,11]. The energy spread of the electron beam is typically about 50–60 eV [12]. The electron density is about 5×10^{12} cm^{-3} and is therefore comparable to that of solar and tokamak plasmas. Unlike other experiments such as those on EBIS sources [13], electron coolers [14], and channeling experiments [15], which have studied dielectronic resonances primarily by observing charged products, EBIT is designed to study electron-ion interactions by observing the x-ray emission.

The first measurement of the $1s2l2l'$ dielectronic resonance strength in a heliumlike ion (Ni^{26+}) from EBIT was recently reported by Knapp *et al.* [12]. In this experiment the x-ray emission was monitored with a solid-state detector, and no individual dielectronic satellite lines were resolved. In the present experiment, dielectronic satellite lines of heliumlike V^{21+} are measured with a crystal spectrometer which has energy resolution of better than 2 eV. Hence we are able to identify individual satellite lines and measure the energy of a given satellite line to within about 0.25–0.50 eV. As the atomic structure of lithiumlike, berylliumlike, and boronlike ions is considerably more complicated than that of heliumlike ions, accurate measurements of the transition energies provide needed data for improving calculational methods. The measurements also provide a first test of relative resonance strengths of individual dielectronic satellite transitions and prepare the way for measurements of dielectronic resonance cross sections that are level specific.

II. THEORY

Dielectronic satellite lines are produced in the radiative stabilization of autoionizing levels populated by the dielectronic capture of a free electron. The production of $K\alpha$ satellite transitions to the heliumlike lines can be schematically expressed as

$$1s^2+e^-\rightarrow 1s2lnl'\rightarrow 1s^2nl'+h\nu_1 . \quad (1)$$

Because the spectator nl' electron perturbs the energy levels only slightly, the energy $h\nu_1$ of the satellite transition is very close to the energy $h\nu_2$ of the heliumlike transition

$$1s2l\rightarrow 1s^2+h\nu_2 . \quad (2)$$

Dielectronic capture is a resonance phenomenon, as the energy of the captured electron must, within the natural resonance width, equal the energy necessary to excite the bound electron. Dielectronic recombination therefore samples only a specific part of the electron distribution function in a plasma. By contrast, dielectronic recombination in EBIT takes place only if the beam energy equals the dielectronic resonance energy. We note that the energy that the free electron must have to produce the photon $h\nu_1$ via the dielectronic process is always less than that necessary for direct excitation, because dielectronic capture involves a change in the ionization state of the ion, i.e., makes use of potential energy associated with the recombining ion.

There are 16 autoionizing lithiumlike levels of the type $1s2l2l'$. These can decay by x-ray emission to one of three lithiumlike ground states, for a total of 22 dipole-allowed x-ray transitions. Similarly, there are 30 autoionizing levels of the type $1s2l^3$ in berylliumlike ions and 35 levels of the type $1s2l^4$ in boronlike ions, which can radi-

atively decay to 10 berylliumlike and 15 boronlike ground levels, respectively. As a result there exist 102 berylliumlike and 217 boronlike dipole-allowed satellite transitions. Only a fraction of these lines have a sufficiently large dielectronic capture cross section and are actually observed.

The emissivity $\epsilon(sf)$ of a dielectronic satellite transition from autoionizing level $|s\rangle$ to lower level $|f\rangle$ is given by the product of the electron density n_e, the density of recombining ions n_{q+1}, and the dielectronic recombination rate α_d,

$$\epsilon(sf)=n_e n_{q+1}\alpha_d \ . \tag{3}$$

Because the electron density is low, we can assume that recombining ions are all in the ground state $|i\rangle$, i.e., that recombination into metastable levels is negligible. The dielectronic recombination rate can be expressed as a product of two terms,

$$\alpha_d=F_1F_2 \ . \tag{4}$$

The first term contains the information about the environment in which dielectronic recombination is observed. The second term is specific to the atomic levels involved and generally is referred to as the line factor [1,2]. In a plasma, F_1 is given by

$$F_1=\frac{1}{2}\left[\frac{2\pi\hbar^2}{mkT_e}\right]^{3/2} e^{-E_{\rm au}/kT_e} \ . \tag{5}$$

$E_{\rm au}$ is the resonance energy for capture of a free electron by the recombining ion in ground state $|i\rangle$ into the autoionizing level $|s\rangle$; T_e, $\hbar$, m, and k are the electron temperature, Planck's constant, the electron mass, and Boltzmann's constant, respectively. In EBIT, where dielectronic recombination takes place in the interaction with an electron beam whose energy spread ΔE at full width at half maximum (FWHM) equals $\Delta E=2\sqrt{\ln 2}\sigma$, F_1 is given by

$$F_1=2\pi^2 a_0^2\left[\frac{I_H}{E_{\rm au}}\right]^{1/2}\frac{I_H}{\sigma\sqrt{\pi}}e^{-(E-E_{\rm au})^2/\sigma^2} \ . \tag{6}$$

Here I_H and a_0 are the Rydberg energy and the Bohr radius, respectively. The line factor F_2 is given by

$$F_2=\frac{g_s}{g_i}\frac{A_a^{si}A_r^{sf}}{\sum_j A_a^{sj}+\sum_{f'}A_r^{sf'}} \ . \tag{7}$$

A_a^{si} is the autoionization rate for decay of upper level $|s\rangle$ to the ground state $|i\rangle$ of the recombining ion; A_r^{sf} is the rate of radiative decay of upper level $|s\rangle$ to lower level $|f\rangle$; g_s and g_i are the statistical weights of the autoionizing level and of the ground state of the recombining ion, respectively. The sum over f' extends over all levels lower than $|s\rangle$; the sum over j extends over all levels which are populated by autoionization of level $|s\rangle$.

The atomic energy levels and bound-state wave functions were calculated using a multiconfigurational Dirac-Fock (MCDF) model in the average-level scheme [16]. The calculations were carried out in intermediate coupling with configuration interaction from the same complex. The effect of the transverse Breit interaction and quantum-electrodynamic corrections were also included in the calculations. Separate MCDF calculations were performed for the initial and final ionic states to determine the transition energies. The Auger and radiative rates were computed according to perturbation theory using the energies and wave functions calculated with the MCDF model [17,18]. These atomic transition rates were then employed to calculate the line factor F_2, Eq. (7). Details of the calculations have been described in Refs. [17] and [18].

III. EXPERIMENT

In EBIT x rays emanate from a narrow, 20-mm-long × 0.06-mm-diam interaction region [10,11]. Thus EBIT represents a line source, and we employ a Bragg crystal spectrometer in the von Hámos geometry to energy analyze the x-ray emission [19].

For the present measurements we used a 12×5-cm^2 Si(220) crystal with a lattice spacing $2d=3.840$ Å bent to a radius of curvature $R=30$ cm. The spectrometer was set to a nominal Bragg angle of 37.5°, which corresponded to a wavelength of $\lambda=2.35$ Å. The total wavelength range covered was $2.27\ \text{Å}<\lambda<2.46\ \text{Å}$. This setting allowed us to view the $n=2$ to $n=1$ spectrum from heliumlike vanadium situated near 2.39 Å concurrently with the Lyα spectrum of hydrogenlike vanadium at 2.28 Å. The plane of dispersion is perpendicular to the direction of the electron beam. Since the crystal acts as a polarizer for Bragg angles near 45°, our setup preferentially records x rays that are polarized parallel to the beam direction.

The two Lyα lines of hydrogenlike vanadium and the $1s2p\ ^1P_1\rightarrow 1s^2\ ^1S_0$ transition in heliumlike vanadium, denoted w by Gabriel [1], served as calibration lines and were used to establish the dispersion of the spectrometer. The wavelengths of Lyα_1 and Lyα_2 were set to $\lambda=2.277\,60$ and $2.283\,02$ Å, respectively, as calculated by Johnson and Soff [20]. The wavelength of w was set to $\lambda=2.381\,87$ Å. This value is 0.000 08 Å lower than the theoretical value given by Drake [21] and 0.000 17 Å lower than the value calculated by Vainshtein and Safronova [22]. We use the lower value because a recent analysis [23] of measured wavelengths of heliumlike resonance lines has indicated that theoretical values for transition elements such as vanadium are usually too large. An interpolation among measured values of w suggests that the wavelength of the heliumlike resonance line calculated by Drake [21] is too large by about 60 ppm, while that of Vainshtein and Safronova [22] is too large by about 125 ppm [23].

The resolving power of our setup is $\lambda/\Delta\lambda=2500$. The center position of each line could be determined with much higher precision, and the uncertainty in the wavelength determination is about 40–80 ppm. X-ray spectra were obtained by setting the energy of the electron beam to a constant value.

IV. DIRECT-EXCITED LINE EMISSION

By setting the beam energy to a value above the threshold for direct electron-impact excitation, we can observe the $n=2$ to $n=1$ spectrum of heliumlike vanadium free of dielectronic satellite lines. Figure 1 shows a typical spectrum obtained at $E=6.85$ keV during a 1-h interval. This value of the beam energy is 1.6 keV above the threshold for excitation of the heliumlike transitions and thus is far from the energy of any dielectronic resonances populating the $n=2$ shell. The spectrum is dominated by four prominent heliumlike lines, which, in addition to the electric dipole transition w include the intercombination lines x and y from levels $1s2p\ ^3P_{2,1}$ and the forbidden line z from level $1s2s\ ^3S_1$. Because the vanadium nucleus has a finite nuclear moment, decay of the $1s2p\ ^3P_0$ level to the $1s^2\ ^1S_0$ ground state is allowed via the hyperfine interaction [24]. This results in a fifth x-ray transition. Its energy, however, is very close to that of y, and the transition cannot be resolved in our observations. The wavelength of the blend, therefore, represents a weighted average of y and $^3P_0$. From calculations of the electron-impact excitation cross sections [25] the intensity of this transition is estimated as one-fourth that of y. Two smaller features are noticeable as well in the spectrum. These correspond to the lithiumlike electric dipole transitions $1s2s2p\ ^2P_{3/2}\rightarrow 1s^22s\ ^2S_{1/2}$ and $1s2s2p\ ^2P_{1/2}\rightarrow 1s^22s\ ^2S_{1/2}$, labeled q and r, respectively. These transitions can in principle be excited by dielectronic recombination. At this beam energy, however, they are excited solely by electron impact. They have the largest inner-shell electron-impact excitation cross section among lithiumlike levels, comparable to those of the heliumlike transitions [25], and the small intensity of q and r relative to the heliumlike transitions indicates that most ions in the trap are in the heliumlike ionization state.

In Table I we list the wavelengths of the observed heliumlike transitions. The measured wavelengths of the two

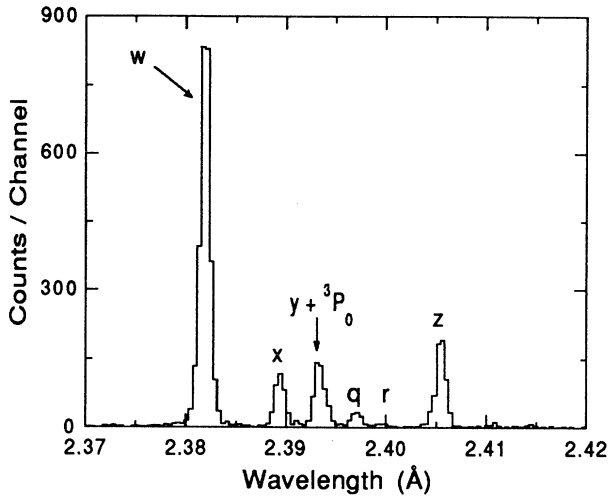

FIG. 1. K spectrum of heliumlike and lithiumlike vanadium in the wavelength region 2.37–2.42 Å showing four heliumlike $n=1$–2 transitions w, x, y, and z and two lithiumlike transitions r and q. Because the vanadium nucleus has a finite nuclear moment, y blends with x rays produced in the hyperfine-induced decay of the $^3P_0$ level. The spectrum was obtained at a beam energy of 6.85 keV in about 60 min of counting time. At this energy no dielectronic resonances are excited that could populate the $n=2$ shell, and all transitions are excited by electron-impact excitation.

electron-impact-excited lithiumlike lines are discussed in Sec. V. The spectrum of heliumlike vanadium has been measured earlier on the TFR tokamak [26]. In the TFR experiment wavelengths were determined relative to a different theoretical value for the wavelength of line w.

TABLE I. Experimental and theoretical wavelengths of the x-ray lines in heliumlike V^{21+}. The theoretical wavelengths of the blend of lines y and $^3P_0$ are estimated assuming that the $^3P_0$ intensity is one-fourth that of y; $\Delta\lambda=\lambda_{theor}-\lambda_{expt}$ denotes the difference between theoretical values and present measurements.

Key	Transition	λ_{expt} [a] (Å)	λ_{expt} [b] (Å)	λ_{theor} [b] (Å)	$\Delta\lambda$ (mÅ)	λ_{theor} [c] (Å)	$\Delta\lambda$ (mÅ)	λ_{theor} [d] (Å)	$\Delta\lambda$ (mÅ)
w	$1s2p\ ^1P_1\rightarrow gs$	2.381 87[e]	2.381 87[e]	2.3787	−3.17	2.382 04	0.17	2.381 95	0.08
x	$1s2p\ ^3P_2\rightarrow gs$	2.389 43(10)	2.389 67	2.3866	−2.83	2.389 57	0.16	2.389 50	0.07
y	$1s2p\ ^3P_1\rightarrow gs$			2.3907		2.393 42		2.393 37	
$^3P_0$	$1s2p\ ^3P_0\rightarrow gs$					2.394 14		2.394 06	
$y,^3P_0$	blend	2.393 38(10)	2.393 67			2.393 56	0.18	2.393 51	0.13
z	$1s2s\ ^3S_1\rightarrow gs$	2.405 64(14)	2.405 87	2.4028	−2.84	2.405 72	0.08	2.405 65	0.03

[a]Present measurement.
[b]TFR Group *et al.*, Ref. [26].
[c]Vainshtein and Safronova, Ref. [22].
[d]Drake, Ref. [21].
[e]Reference line; wavelength set to the semiempirical value of 2.381 87 Å.

For better comparison we have normalized the TFR values to the theoretical value of line w that we used in our measurement.

Spectra observed from plasma sources generally contain a mixture of lines excited by electron collisions and dielectric recombination, and every heliumlike line blends to some extent with one or more dielectronic satellite lines. Systematic line broadening and shifts of line w due to such blends have been investigated by Bitter *et al.* [27]. Because the intensities of lines x, y, and z are much smaller than that of line w in plasma spectra and, more importantly, are on the order of the intensities of dielectronic satellite lines, their measured wavelengths are potentially more uncertain. In the present measurement we have observed the heliumlike lines free of blends with dielectronic satellite lines. The accuracy of our measurement is, therefore, limited by the resolution of the spectrometer and uncertainties in the dispersion. The experimental error is estimated to be about 0.1 mÅ, or 40–60 ppm, and is largest for z, because the line is furthest away from w. A comparison of our results with those obtained on the TFR tokamak [26] shows differences ranging between 0.2 and 0.3 mÅ for x, y, and z.

In Table I we also list values computed by the TFR Group *et al.* [26] using a multiconfigurational intermediate coupling scheme, by Vainshtein and Safronova [22] using the Z-expansion method, and by Drake [21], who uses a nonrelativistic variational technique. Best agreement is found with the computed values of Drake. The differences are around 0.1 mÅ and are insignificant when error limits are taken into account. The values of Vainshtein and Safronova agree slightly less well with the experimental values than those of Drake. The largest differences are found for the values of the TFR Group *et al.;* their values are too small by 2.8–3.2 mÅ. Evidently, better agreement with theoretical values would have been achieved if we had normalized the wavelength of w to that of the respective calculation.

V. *KLL* SATELLITE SPECTRA

Electrons with kinetic energies between 3550 and 3670 eV dielectronically recombine with heliumlike vanadium ions into lithiumlike autoionizing configurations $1s2l2l'$ (cf. Table II). At somewhat higher energies, electrons recombine with lithiumlike and berylliumlike ions (cf. Tables III and IV). Tuning the electron beam to the appropriate resonance energies we have observed a set of x-ray spectra that allows us to identify the principal dielectronic satellite transitions. The energy spread of the electron beam in the present experiment is about 100-eV FWHM. The spread results from the space charge of the electrons and from ripple in the high-voltage power supply used to accelerate beam electrons. Because many dielectronic resonances are spaced closer together than the spread in beam energy, several resonances may be excited concurrently in a single setting of the electron beam, and more than one dielectronic satellite transition can usually be observed. Setting the beam energy equal to that of a given resonance results, of course, in a much more intense dielectronic satellite line than the line intensity that results from the interaction of the same resonance with electrons in the wings of the beam energy distribution.

Spectra of the *KLL* dielectronic satellite transitions observed at three different electron beam energies are shown in Figs. 2(a)–2(c). The integration time for each

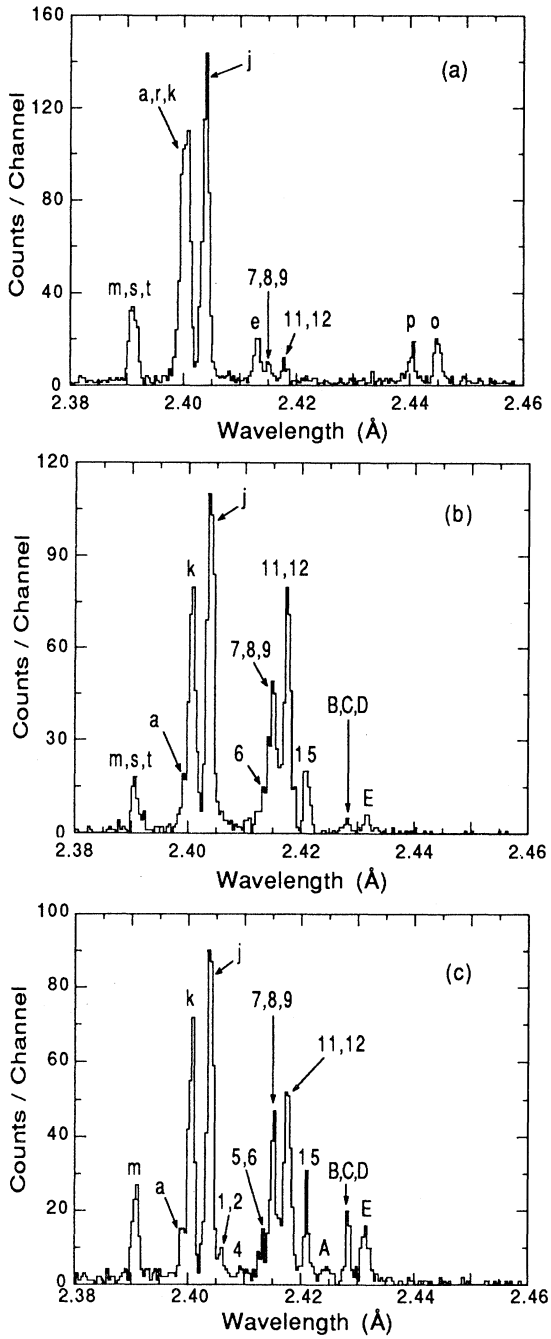

FIG. 2. *KLL* satellite spectra of V^{21+}. The beam energy was set to (a) 3580, (b) 3700, and (c) 3740 eV. At the lower energy satellites composed of transitions in lithiumlike ions, identified with lowercase letters, dominate. Satellites from berylliumlike (numerals) and boronlike (uppercase letters) ions are more prominent at higher energies.

TABLE II. Atomic data for the dielectronic satellite transitions $1s^2 2l$-$1s 2l^2$ in lithiumlike V^{20+}. Transitions are labeled in the notation of Gabriel (Ref. [1]). $\sum_j A_a^{sj} = A_a^{si}$ and is not listed. Experimental wavelengths are measured with respect to the heliumlike reference line w with wavelength set to the semiempirical value of 2.381 87 Å. The theoretical wavelengths of the blend s and t are estimated based on their respective line factors. $\Delta\lambda = \lambda_{\text{theor}} - \lambda_{\text{expt}}$ denotes the difference between theoretical values and present measurements. $a[b] = a \times 10^b$.

Key	Transition	E_{au} (eV)	A_a^{si} (s^{-1})	A_r^{sf} (s^{-1})	F_2 (s^{-1})	λ_{expt} [a] (Å)	λ_{expt} [b] (Å)	λ_{theor} [c] (Å)	$\Delta\lambda$ (mÅ)	λ_{theor} [d] (Å)	$\Delta\lambda$ (mÅ)
a	$(1s2p_{3/2}^2)_{3/2} \rightarrow 1s^2 2p_{3/2}$	3649.7	2.81[+13]	3.35[+14]	1.01[+14]	2.3990(2)	⟨2.4004⟩[e]	2.3993	+0.3	2.3986	−0.4
b	$(1s2p_{1/2}^2)_{3/2} \rightarrow 1s^2 2p_{1/2}$	3649.7	2.81[+13]	7.40[+12]	2.24[+12]			2.3950		2.3943	
c	$(1s2p_{1/2}2p_{3/2})_{1/2} \rightarrow 1s^2 2p_{3/2}$	3639.4	7.23[+11]	9.75[+13]	3.65[+11]			2.4041		2.4033	
d	$(1s2p_{/2}2p_{3/2})_{1/2} \rightarrow 1s^2 2p_{1/2}$	3639.4	7.23[+11]	2.88[+14]	1.08[+12]			2.3998		2.3990	
e	$(1s2p_{1/2}2p_{3/2})_{5/2} \rightarrow 1s^2 p_{3/2}$	3619.5	1.05[+13]	9.00[+12]	2.91[+13]	2.4130(2)		2.4134	+0.4	2.4124	−0.6
f	$(1s2p_{1/2}2p_{3/2})_{3/2} \rightarrow 1s^2 2p_{3/2}$	3615.4	2.51[+11]	3.35[+12]	1.65[+12]			2.4154		2.4138	
g	$(1s2p_{1/2}2p_{3/2})_{3/2} \rightarrow 1s^2 2p_{1/2}$	3615.4	4.74[+11]	1.26[+10]	6.21[+9]			2.4110		2.4100	
h	$(1s2p_{1/2}^2)_{1/2} \rightarrow 1s^2 2p_{3/2}$	3610.9	1.61[+11]	7.40[+10]	4.36[+9]			2.4175		2.4164	
i	$(1s2p_{1/2}^2)_{1/2} \rightarrow 1s^2 2p_{3/2}$	3610.9	1.61[+11]	5.25[+12]	3.09[+11]			2.4131		2.4120	
j	$(1s2p_{3/2}^2)_{5/2} \rightarrow 1s^2 2p_{3/2}$	3640.0	1.45[+14]	1.24[+14]	4.00[+14]	2.4038(2)	2.4042	2.4038	0.0	2.4033	−0.5
k	$(1s2p_{1/2}2p_{3/2})_{3/2} \rightarrow 1s^2 2p_{1/2}$	3637.7	1.29[+14]	1.68[+14]	2.78[+14]	2.4006(2)	⟨2.4004⟩[e]	2.4006	0.0	2.4000	−0.6
l	$(1s2p_{1/2}2p_{3/2})_{3/2} \rightarrow 1s^2 2p_{3/2}$	3637.7	1.29[+14]	1.43[+13]	2.37[+13]			2.4049		2.4043	
m	$(1s2p_{3/2}^2)_{1/2} \rightarrow 1s^2 2p_{3/2}$	3669.5	2.70[+13]	1.18[+14]	4.07[+13]	2.3906(3)		2.3902	−0.4	2.3900	−0.6
n	$(1s2p_{3/2}^2)_{1/2} \rightarrow 1s^2 p_{1/2}$	3669.5	2.70[+13]	1.17[+13]	4.02[+12]			2.3859		2.3858	
o	$(1s2s^2)_{1/2} \rightarrow 1s^2 2p_{3/2}$	3550.7	1.24[+14]	5.68[+12]	1.05[+13]	2.4450(2)		2.4462	+1.2	2.4446	−0.4
p	$(1s2s^2)_{1/2} \rightarrow 1s^2 2p_{1/2}$	3550.7	1.24[+14]	4.61[+12]	8.51[+12]	2.4403(2)		2.4417	+1.4	2.4401	−0.2
q	$(1s2s2p_{3/2})_{3/2} \rightarrow 1s^2 2s_{1/2}$	3601.1	2.10[+12]	2.51[+14]	8.32[+12]	2.3970(1)	2.3973	2.3979	+0.9	2.3966	−0.4
r	$(1s2s2p_{1/2})_{1/2} \rightarrow 1s^2 2s_{1/2}$	3595.1	2.89[+13]	1.84[+14]	5.00[+13]	2.3993(2)	⟨2.4004⟩[e]	2.4007	+1.4	2.3989	−0.4
s	$(1s2s2p_{3/2})_{3/2} \rightarrow 1s^2 2s_{1/2}$	3616.7	9.46[+13]	9.94[+12]	3.60[+13]			2.3907		2.3899	
t	$(1s2s2p_{3/2})_{1/2} \rightarrow 1s^2 2s_{1/2}$	3615.5	7.57[+13]	7.99[+13]	7.77[+13]			2.3912		2.3908	
s,t						2.3912(2)		2.3910	−0.2	2.3905	−0.7
u	$(1s2s2p_{1/2})_{3/2} \rightarrow 1s^2 2s_{1/2}$	3564.5	2.51[+11]	4.70[+12]	9.51[+11]			2.4150		2.4143	
v	$(1s2s2p_{1/2})_{1/2} \rightarrow 1s^2 2s_{1/2}$	3562.1	2.67[+10]	1.59[+12]	5.25[+10]			2.4161		2.4149	

[a] Present measurement.
[b] TFR Group *et al.*, Ref. [26].
[c] Present MCDF calculations.
[d] Vainshtein and Safronova, Ref. [31].
[e] Blend of lines a, r, and k.

TABLE III. Atomic data for the principal dielectronic satellite transitions $1s^2 2l^2$-$1s2l^3$ in berylliumlike V^{19+}. Only transitions with line factor F_2 larger than 4×10^{12} s^{-1} are listed. Experimental wavelengths are measured with respect to the heliumlike line w set to the semiempirical value of 2.381 87 Å. ⟨ ⟩ denotes blends. $a[b]=a\times10^{b}$.

Key	Transition	λ_{theor} (Å)	λ_{expt} (Å)	E_{au} (eV)	A_a^{si} (s^{-1})	$\sum_j A_a^{sj}$ (s^{-1})	A_r^{sf} (s^{-1})	F_2 (s^{-1})
1	$(1s2s2p_{3/2}^2)_1\rightarrow(1s^22s2p_{3/2})_2$	2.4050	⟨2.4060(3)⟩	3714.9	1.88[+13]	1.01[+14]	6.12[+13]	1.04[+13]
2	$(1s2s2p_{1/2}^2)_1\rightarrow(1s^22s2p_{1/2})_1$	2.4066	⟨2.4060(3)⟩	3704.9	4.29[+13]	9.46[+13]	3.14[+13]	1.12[+13]
3	$(1s2s2p_{1/2}2p_{3/2})_2\rightarrow(1s^22s2p_{3/2})_2$	2.4075		3709.6	1.16[+14]	2.29[+14]	2.13[+13]	7.17[+12]
4	$(1s2s2p_{1/2}^2)_1\rightarrow(1s^22s2p_{3/2})_2$	2.4097	2.4100(4)	3769.3	4.29[+13]	9.46[+13]	3.97[+13]	1.42[+13]
5	$(1s2s2p_{3/2}^2)_0\rightarrow(1s^22s2p_{3/2})_1$	2.4126	⟨2.4130(2)⟩	3731.6	5.80[+13]	1.78[+14]	1.04[+14]	1.07[+13]
6	$(1s2s2p_{1/2}2p_{3/2})_1\rightarrow(1s^22s2p_{1/2})_0$	2.4129	⟨2.4130(2)⟩	3689.0	1.26[+14]	1.44[+14]	2.11[+13]	9.85[+12]
7	$(1s2s2p_{1/2}2p_{3/2})_1\rightarrow(1s^22s2p_{1/2})_1$	2.4141	⟨2.4151(2)⟩	3689.0	1.26[+14]	1.44[+14]	8.58[+13]	4.00[+13]
8	$(1s2s2p_{1/2}2p_{3/2})_2\rightarrow(1s^22s2p_{1/2})_1$	2.4157	⟨2.4151(1)⟩	3685.7	8.26[+13]	9.66[+13]	1.67[+14]	8.94[+13]
9	$(1s2s2p_{3/2}^2)_2\rightarrow(1s^22s2p_{3/2})_2$	2.4162	⟨2.4151(1)⟩	3691.1	6.35[+13]	9.45[+13]	2.05[+14]	1.07[+14]
10	$(1s2s2p_{1/2}2p_{3/2})_1\rightarrow(1s^22s2p_{3/2})_2$	2.4171		3689.0	1.26[+14]	1.44[+14]	1.91[+13]	8.88[+12]
11	$(1s2s2p_{1/2}2p_{3/2})_3\rightarrow(1s^22s2p_{3/2})_2$	2.4175	⟨2.4176(2)⟩	3688.3	1.42[+14]	1.55[+14]	1.11[+14]	1.19[+14]
12	$(1s2s2p_{1/2}2p_{3/2})_2\rightarrow(1s^22s2p_{3/2})_2$	2.4187	⟨2.4176(2)⟩	3685.7	8.23[+13]	9.66[+13]	4.39[+13]	2.36[+13]
13	$(1s2s2p_{3/2}^2)_2\rightarrow(1s^22s2p_{3/2})_1$	2.4189		3718.2	2.30[+13]	1.48[+14]	1.55[+13]	5.07[+12]
14	$1s2s2p_{1/2}2p_{3/2})_1\rightarrow(1s^22s2p_{3/2})_2$	2.4201		3682.6	1.55[+13]	4.23[+13]	8.75[+13]	4.00[+12]
15	$(1s2s2p_{1/2}2p_{3/2})_2\rightarrow(1s^22s2p_{3/2})_1$	2.4230	2.4210(2)	3709.6	1.16[+14]	2.29[+14]	9.36[+13]	3.15[+13]
16	$(1s2s^22p_{1/2})\rightarrow(1s^22p_{1/2}^2)_0$	2.4235		3628.9	5.26[+13]	1.45[+14]	1.17[+13]	5.71[+12]
17	$(1s2s2p_{3/2}^2)_3\rightarrow(1s^22s2p_{3/2})_2$	2.4349		3651.6	2.58[+12]	2.70[+12]	2.22[+12]	4.07[+12]

spectrum is about 20 min, and the data in Fig. 2 represent only a fraction of the data recorded, as we scanned the *KLL* resonance in 20–40-eV steps.

The satellite transitions *o* and *p* correspond to the lowest-energy dielectronic resonance involving *K*-shell electrons. Setting the electron beam to a value near their resonance energy, we can observe these transitions distinctly despite their small cross sections, as demonstrated by the spectrum in Fig. 2(a). Note the two-electron, one-photon nature of *o* and *p*. These transitions arise from the radiative decay of the $1s2s^2$ level to lower levels $1s^22p_{1/2}$ and $1s^22p_{1/2}$ (cf. Table II). In single-configuration calculations such radiative decay is forbidden, and autoionization is the only decay mode. Radiative decay of this level is enabled because it admixes with the $1s2p^2$ configuration. In plasma-produced spectra the two satellite lines *o* and *p* typically blend with lines from other ionization states (*o* and *p* in iron, for example, have been found to blend with transitions in carbonlike iron [28,29]) and therefore have never been identified. Because of the spread in beam energy other lithiumlike satellite transitions are excited at this beam energy as well, and are seen in Fig. 2(a). Most notable are the strong dielectronic satellites *j* and *k*. These have previously been identified in all high-resolution x-ray spectra of the transition metals from low-density plasma sources [26,30]. Transition *e*, on the other hand, like *o* and *p*, has never before been seen.

As the energy of the electron beam is increased, the relative intensity of the satellite lines changes. This allows us to identify the contributions of individual satellite lines that blend, such as *r* and *a*. Raising the beam energy to 3700 eV dielectronic satellite transitions from autoionizing levels $1s2l^3$ in berylliumlike vanadium are excited, as shown in Fig. 2(b). Increasing the beam energy by an additional 40 eV, boronlike satellite transitions involving levels $1s2l^4$ prominently contribute to the spectral line emission.

The measured transition energies of the satellites from lithiumlike ions are given in Table II. The values for the wavelengths of *r* and *q* have been determined from spectra excited by electron impact, as discussed in Sec. IV. The line factor of *q* is very small, and this line has not been resolved in the satellite spectra. On the other hand, the line factor of *r* is large; however, *r* blends with *a*. Knowledge of its position from the direct-excited spectra has been used to resolve the blend and to determine the wavelength of *a*. The experimental wavelengths are compared with values calculated with the MCDF code and those calculated by Vainshtein and Safronova [31] using the *Z*-expansion method. The latter calculation appears to give the best agreement with the data; theoretical values are consistently too low by 0.2–0.7 mÅ. The MCDF values differ by larger amounts, which range between −0.4 and +1.4 mÅ. The errors in the MCDF values can be traced to the use of the average-level scheme and the neglect of the ground-state correlation correction. The wavelengths of *q* and *j* have previously been measured by the TFR Group *et al.* [26]. Their values are somewhat larger than ours (+0.3 and +0.4 mÅ, respectively).

TABLE IV. Atomic data for the principal dielectronic satellite transitions $1s^22l^3$-$1s2l^4$ in boronlike V^{18+}. Only transitions with line factor F_2 larger than 4×10^{12} s^{-1} are listed. Experimental wavelengths are measured with respect to the heliumlike reference line *w* set to the semiempirical value of 2.381 87 Å. ⟨ ⟩ denotes blends. $a[b]=a\times10^b$.

Key	Transition	λ_{theor} (Å)	λ_{expt} (Å)	E_{au} (eV)	A_a^{si} (s^{-1})	$\sum_j A_a^{sj}$ (s^{-1})	A_r^{sf} (s^{-1})	F_2 (s^{-1})
A	$(1s2s^2p_{3/2}^2)_{1/2}\rightarrow 1s^22s^22p_{3/2}$	2.4249	2.4244(5)	3768.6	8.12[+13]	2.81[+14]	1.57[+14]	5.75[+13]
B	$(1s2s^22p_{3/2}^2)_{3/2}\rightarrow 1s^22s^22p_{3/2}$	2.4274	⟨2.4282(2)⟩	3763.4	2.28[+13]	1.79[+14]	3.24[+14]	5.71[+13]
C	$(1s2s^22p_{1/2}2p_{3/2})_{1/2}\rightarrow 1s^22s^22p_{1/2}$	2.4282	⟨2.4282(2)⟩	3753.1	1.18[+13]	1.65[+14]	2.92[+14]	1.31[+13]
D	$(1s2s^22p_{1/2}2p_{3/2})_{3/2}\rightarrow 1s^22s^22p_{1/2}$	2.4285	⟨2.4282(2)⟩	3752.5	1.11[+14]	3.11[+14]	1.63[+14]	1.47[+14]
E	$(1s2s^22p_{3/2}^2)_{5/2}\rightarrow 1s^22s^22p_{3/2}$	2.4316	2.4315(3)	3754.5	1.29[+14]	3.46[+14]	1.20[+14]	1.98[+14]
F	$(1s2s^22p_{1/2}2p_{3/2})_{3/2}\rightarrow 1s^22s^22p_{3/2}$	2.4326		3752.5	1.11[+14]	3.11[+14]	1.40[+13]	1.26[+13]
G	$(1s2s^22p_{3/2}^2)_{5/2}\rightarrow(1s^22p_{1/2}2p_{3/2}^2)_{5/2}$	2.4990		3754.5	1.29[+14]	3.46[+14]	2.86[+12]	4.70[+12]

In Table III we list the experimental transition energies of the dielectronic satellite lines from berylliumlike ions. A total of six features are observed that are ascribed to transitions in berylliumlike vanadium. Identifications are made based on predicted intensities and line positions. Most observed features are blends of several lines.

The experimental wavelengths of the dielectronic satellite lines from boronlike ions are listed in Table IV. The dielectronic satellite spectrum composed of boronlike transitions is less complex than that formed by lithiumlike or berylliumlike transitions. Although there are 217 dipole-allowed dielectronic satellite transitions in boronlike ions, only seven transitions have a line factor larger than 1% that of satellite j in lithiumlike ions. Three features are identified in the observations which correspond to five of the transitions listed in Table IV. A comparison between measured and predicted wavelengths shows agreement within the experimental error bars.

VI. *KLM* SATELLITE SPECTRA

Dielectronic satellite lines with an $n=3$ spectator electron have been extensively modeled in high-resolution spectra from the sun [2,32,33] and tokamaks [34–36]. Although individual satellite lines are closely clustered and cannot be resolved, they form features which can be easily identified in most spectra. In vanadium the *KLM* dielectronic resonances, involving configurations of the type $1s2l3l'$, occur for electron energies between 4450 and 4540 eV. This is about 900 eV higher than $n=2$ resonances. Hence, in a plasma *KLM* resonances sample a different part of a given electron distribution function than *KLL* resonances, and a comparison between $n=3$ and $n=2$ satellite lines provides information about the shape of the electron distribution. This property has been used in various investigations of tokamak plasmas [5,6] and solar flares [7] to ascertain the existence of non-Maxwellian electron distributions.

X-ray spectra observed at two beam energies, 4440 and 4510 eV, are shown in Figs. 3(a) and 3(b). The observed satellite lines can be grouped into three broad features, which are labeled $3A$, $3B$, and $3C$ in Fig. 3(b). The first is situated near 2.385 Å and consists entirely of satellite lines from lithiumlike ions (cf. Table V). This feature falls into a wavelength region between the location of w and x, which is devoid of any other lines even in plasma observations. A second grouping of satellite lines from lithiumlike ions forms the feature $3B$ centered at 2.393 Å. The feature labeled $3C$ consists mostly of a cluster of satellite lines from berylliumlike ions (cf. Table VI), augmented by several weak satellite lines from lithiumlike ions. In the spectrum shown in Fig. 3(a) we can identify two additional features labeled $3o$ and $3p$. These are close analogs of the $n=2$ satellites o and p in lithiumlike ions. As is the case for their $n=2$ counterparts, we find that the calculated wavelengths are too long by about 1.0 mÅ.

TABLE V. Atomic data for the principal dielectronic satellite transitions $1s^2 3l$-$1s2l3l'$ in lithiumlike V^{20+}. Only transitions with line factor F_2 larger than 4×10^{12} s^{-1} are listed. Experimental wavelengths are measured with respect to the heliumlike reference line w set to the semiempirical value of 2.381 87 Å. $\sum_j A_a^{sj}=A_a^{si}$ and is not listed. ⟨ ⟩ denotes blends. $a[b]=a\times10^b$.

Key	Transition	λ_{theor} (Å)	λ_{expt} (Å)	E_{au} (eV)	A_a^{si} (s^{-1})	A_r^{sf} (s^{-1})	F_2 (s^{-1})
$3A$	$(1s2p_{3/2}3d_{3/2})_{5/2}\rightarrow 1s^2 3d_{3/2}$	2.3823	⟨2.385⟩	4536.2	1.35[+13]	1.46[+14]	5.06[+13]
$3A$	$(1s2p_{3/2}3d_{3/2})_{5/2}\rightarrow 1s^2 3d_{5/2}$	2.3827	⟨2.385⟩	4536.2	1.35[+13]	7.36[+13]	2.56[+13]
$3A$	$(1s2p_{3/2}3p_{3/2})_{1/2}\rightarrow 1s^2 3p_{3/2}$	2.3829	⟨2.385⟩	4530.5	1.25[+13]	1.85[+14]	2.08[+13]
$3A$	$(1s2p_{3/2}3d_{5/2})_{7/2}\rightarrow 1s^2 3d_{5/2}$	2.3838	⟨2.385⟩	4534.0	1.44[+13]	2.32[+14]	1.09[+14]
$3A$	$(1s2p_{3/2}3d_{5/2})_{5/2}\rightarrow 1s^2 3d_{5/2}$	2.3848	⟨2.385⟩	4532.4	1.59[+12]	1.82[+14]	6.40[+12]
$3A$	$(1s2p_{3/2}3s)_{1/2}\rightarrow 1s^2 3s$	2.3848	⟨2.385⟩	4511.8	1.05[+13]	2.27[+14]	1.98[+13]
$3A$	$(1s2p_{3/2}3s)_{3/2}\rightarrow 1s^2 3s$	2.3852	⟨2.385⟩	4511.2	2.31[+12]	2.30[+14]	8.99[+12]
$3A$	$(1s2p_{3/2}3p_{3/2})_{3/2}\rightarrow 1s^2 3p_{3/2}$	2.3854	⟨2.385⟩	4525.2	1.66[+13]	2.39[+14]	5.70[+13]
$3A$	$(1s2p_{3/2}3p_{1/2})_{3/2}\rightarrow 1s^2 3p_{1/2}$	2.3855	⟨2.385⟩	4522.0	3.10[+13]	2.32[+14]	1.03[+14]
$3A$	$(1s2p_{3/2}3p_{3/2})_{5/2}\rightarrow 1s^2 p_{3/2}$	2.3862	⟨2.385⟩	4523.3	3.03[+13]	2.47[+14]	1.57[+14]
$3B$	$(1s2p_{3/2}3s)_{3/2}\rightarrow 1s^2 3s$	2.3893	⟨2.392⟩	4502.4	3.90[+13]	1.88[+12]	7.11[+12]
$3B$	$(1s2p_{3/2}3p_{3/2})_{5/2}\rightarrow 1s^2 3p_{3/2}$	2.3915	⟨2.392⟩	4511.9	2.97[+13]	9.05[+12]	1.77[+13]
$3B$	$(1s2p_{1/2}3s)_{1/2}\rightarrow 1s^2 3s$	2.3930	⟨2.392⟩	4494.1	3.82[+13]	4.20[+13]	3.96[+13]
$3B$	$(1s2p_{3/2}3p_{3/2})_{3/2}\rightarrow 1s^2 3p_{3/2}$	2.3941	⟨2.392⟩	4506.3	9.37[+12]	1.91[+13]	1.13[+13]
$3B$	$(1s2p_{3/2}3p_{1/2})_{5/2}\rightarrow 1s^2 3p_{3/2}$	2.3949	⟨2.392⟩	4504.4	3.84[+12]	9.78[+12]	1.49[+13]
$3C$	$(1s2p_{1/2}3d_{5/2})_{7/2}\rightarrow 1s^2 3d_{5/2}$	2.3969	⟨2.400⟩	4505.4	5.48[+11]	8.55[+12]	4.12[+12]
$3C$	$(1s2p_{1/2}3p_{3/2})_{5/2}\rightarrow 1s^2 3p_{3/2}$	2.3990	⟨2.400⟩	4495.6	1.77[+12]	1.15[+13]	9.18[+12]
$3p$	$(1s2s3s)_{1/2}\rightarrow 1s^2 3p_{1/2}$	2.4051	2.4040(5)	4479.1	2.13[+13]	6.89[+12]	7.45[+12]
$3o$	$(1s2s3s)_{1/2}\rightarrow 1s^2 3p_{3/2}$	2.4064	2.4052(5)	4479.1	2.13[+13]	1.05[+13]	1.13[+13]

VII. HIGH-n SATELLITE SPECTRA

Heliumlike dielectronic resonances with $n=4,5,6$ are found at electron energies between 4760 and 4830, 4905 and 4965, and 4985 and 5035 eV, respectively. The resulting satellite transitions form two distinct groups of lines located near the position of heliumlike lines w and y. In plasma observations they cause a broadening and shift of the apparent lines w and y [27,33–35].

The satellite intensity depends on the product of the autoionization rate and the radiative decay rate, Eq. (7). Autoionization rates scale as n^{-3} [37]. For example, the maximum autoionization rate falls from 1.45×10^{14} s^{-1} for $n=2$ (Table II) to 3.20×10^{12} s^{-1} for $n=6$ (Table VII) for lithiumlike ions. As a result, the dielectronic capture rate decreases, and high-n satellites are progres-

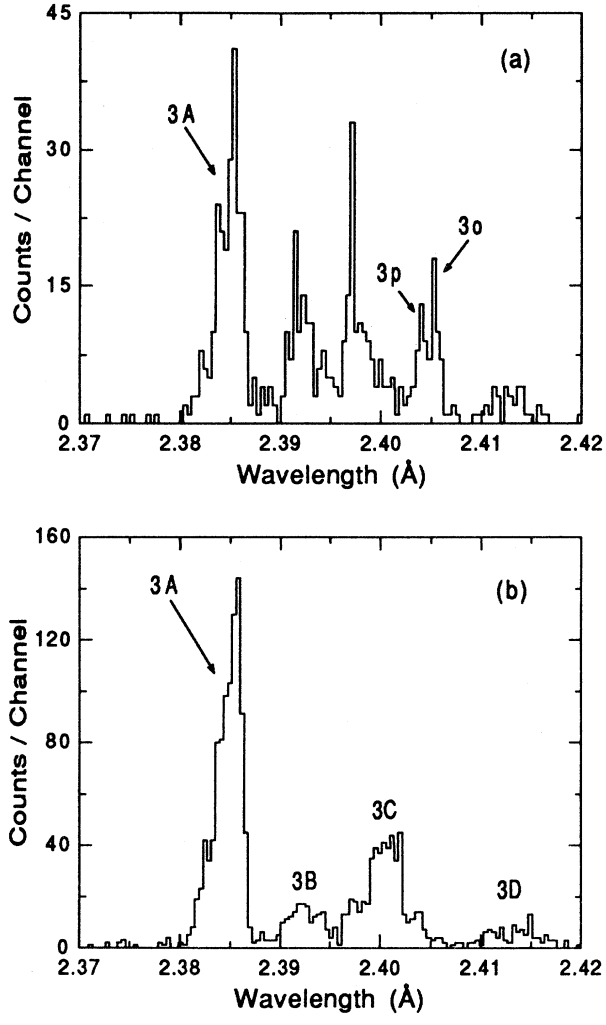

FIG. 3. *KLM* satellite spectra of V^{21+}. The beam energy was set to (a) 4440 and (b) 4510 eV. The features labeled $3A$ and $3B$ consist of satellite lines from lithiumlike ions, $3C$ consists predominantly of satellite lines from berylliumlike ions.

TABLE VI. Atomic data for the principal dielectronic satellite transitions $1s^22l3l'$-$1s2l^23l'$ in berylliumlike V^{19+}. Only transitions with line factor $F_2\geq4\times10^{12}$ s^{-1} are listed. Experimental wavelengths are measured with respect to the heliumlike reference line w set to the semiempirical value of 2.381 87 Å. $\langle\ \rangle$ denotes blends. $a[b]=a\times10^{b}$.

Key	Transition	λ_{theor} (Å)	λ_{expt} (Å)	E_{au} (eV)	A_a^{si} (s^{-1})	$\sum_j A_a^{sj}$ (s^{-1})	A_r^{sf} (s^{-1})	F_2 (s^{-1})
3C	$(1s2s2p_{3/2}3s)_1\rightarrow(1s^22s3s)_0$	2.3952	$\langle2.400\rangle$	4540.2	1.38[+13]	2.38[+14]	3.17[+13]	5.66[+12]
3C	$(1s2s2p_{3/2}3p_{1/2})_1\rightarrow(1s^22s3p_{1/2})_1$	2.3958	$\langle2.400\rangle$	4549.3	2.49[+13]	1.56[+14]	4.52[+13]	5.61[+12]
3C	$(1s2s2p_{3/2}3p_{1/2})_1\rightarrow(1s^22s3p_{1/2})_0$	2.3959	$\langle2.400\rangle$	4549.3	2.49[+13]	1.56[+14]	3.53[+13]	4.38[+12]
3C	$(1s2s2p_{3/2}3p_{3/2})_0\rightarrow(1s^22s3p_{1/2})_1$	2.3983	$\langle2.400\rangle$	4544.0	8.24[+12]	2.45[+13]	6.46[+13]	4.17[+12]
3C	$(1s2s2p_{3/2}3p_{3/2})_0\rightarrow(1s^22s3p_{3/2})_1$	2.3993	$\langle2.400\rangle$	4544.0	8.24[+12]	2.45[+13]	1.39[+13]	8.99[+12]
3C	$(1s2s2p_{3/2}3d_{5/2})_4\rightarrow(1s^22s3d_{5/2})_3$	2.3997	$\langle2.400\rangle$	4554.1	1.06[+13]	1.00[+14]	2.29[+14]	1.94[+13]
3C	$(1s2s2p_{3/2}3d_{3/2})_3\rightarrow(1s^22s3d_{5/2})_2$	2.4005	$\langle2.400\rangle$	4559.6	7.81[+12]	1.50[+14]	2.05[+14]	1.23[+13]
3C	$(1s2s2p_{3/2}3p_{1/2})_2\rightarrow(1s^22s3p_{1/2})_1$	2.4011	$\langle2.400\rangle$	4538.0	3.14[+13]	1.01[+14]	1.92[+14]	2.93[+13]
3C	$(1s2s2p_{3/2}3p_{3/2})_1\rightarrow(1s^22s3p_{3/2})_1$	2.4012	$\langle2.400\rangle$	4540.1	5.79[+12]	1.14[+14]	1.12[+14]	5.08[+12]
3C	$(1s2s2p_{3/2}3p_{3/2})_3\rightarrow(1s^22s3p_{3/2})_2$	2.4022	$\langle2.400\rangle$	4538.2	1.53[+13]	6.82[+13]	2.40[+14]	2.49[+13]
3C	$(1s2p_{1/2}2p_{3/2}3s)_0\rightarrow(1s^22p_{1/2}3s)_1$	2.4025	$\langle2.400\rangle$	4566.1	6.78[+12]	6.19[+13]	1.93[+14]	4.76[+12]
3C	$(1s2s2p_{3/2}3p_{3/2})_0\rightarrow(1s^22p_{1/2}3s)_1$	2.4030	$\langle2.400\rangle$	4565.1	8.81[+12]	7.67[+13]	1.22[+14]	8.44[+12]
3D	$(1s2s2p_{3/2}3p_{3/2})_2\rightarrow(1s^22s3p_{3/2})_2$	2.4150		4510.8	2.24[+13]	8.96[+13]	4.87[+12]	4.22[+12]

sively less intense than those of the *KLL* or *KLM* resonances. Moreover, only those high-n autoionizing levels that have radiative rates that are larger than the autoionizing rates produce strong satellite lines. The radiative rate of the $n=2$ electron can be approximated by that of its spectator-free-parent line because the high-n spectator electron represents only a small perturbation. Among the heliumlike parent lines only the dipole-allowed transitions w and y have radiative rates exceeding the Auger rates of the lithiumlike high-n levels with $n \leq 6$ [38]. Heliumlike lines x and z are dipole forbidden and have transition rates less than 10^{11} s^{-1} [38]. Consequently,

TABLE VII. Atomic data for the principal dielectronic satellite transitions $1s^2nl$-$1s2lnl'$ in lithiumlike V^{21+} with $n=4,5,6$. Only transitions with line factor $F_2 \geq 4\times10^{12}$ s^{-1} are listed. Experimental wavelengths are measured with respect to the heliumlike reference line w set to the semiempirical value of 2.381 87 Å. ⟨ ⟩ denotes blends. $\sum_j A_a^{sj} = A_a^{si}$ and is not listed. $a[b]=a\times10^b$.

Key	Transition	λ_{theor} (Å)	λ_{expt} (Å)	E_{au} (eV)	A_a^{si} (s^{-1})	A_r^{sf} (s^{-1})	F_2 (s^{-1})
			$n=4$				
4*A*	$(1s2p_{3/2}4f_{7/2})_{9/2}\rightarrow 1s^24f_{7/2}$	2.3823	⟨2.383⟩	4829.2	4.39[+11]	2.72[+14]	4.37[+12]
4*A*	$(1s2p_{3/2}4d_{5/2})_{5/2}\rightarrow 1s^24d_{3/2}$	2.3828	⟨2.383⟩	4827.6	5.97[+12]	1.30[+14]	1.75[+13]
4*A*	$(1s2p_{3/2}4d_{5/2})_{5/2}\rightarrow 1s^24d_{5/2}$	2.3829	⟨2.383⟩	4827.6	5.97[+12]	1.30[+14]	1.75[+13]
4*A*	$(1s2p_{3/2}4p_{3/2})_{1/2}\rightarrow 1s^24p_{3/2}$	2.3831	⟨2.383⟩	4825.2	4.88[+12]	2.26[+14]	8.11[+12]
4*A*	$(1s2p_{3/2}4d_{3/2})_{5/2}\rightarrow 1s^24d_{3/2}$	2.3831	⟨2.383⟩	4826.8	1.68[+12]	1.34[+14]	4.96[+12]
4*A*	$(1s2p_{3/2}4d_{3/2})_{5/2}\rightarrow 1s^24d_{5/2}$	2.3833	⟨2.383⟩	4826.8	1.68[+12]	1.36[+14]	5.05[+12]
4*A*	$(1s2p_{3/2}4d_{5/2})_{7/2}\rightarrow 1s^24d_{5/2}$	2.3833	⟨2.383⟩	4826.8	6.64[+12]	2.72[+14]	5.19[+13]
4*A*	$(1s2p_{3/2}4p_{3/2})_{3/2}\rightarrow 1s^24d_{3/2}$	2.3838	⟨2.383⟩	4818.2	3.69[+12]	2.65[+14]	1.41[+13]
4*A*	$(1s2p_{3/2}4p_{1/2})_{3/2}\rightarrow 1s^24p_{1/2}$	2.3838	⟨2.383⟩	4822.3	1.17[+13]	2.64[+14]	4.39[+13]
4*A*	$(1s2p_{3/2}4p_{3/2})_{5/2}\rightarrow 1s^24d_{3/2}$	2.3840	⟨2.383⟩	4823.1	8.10[+12]	2.70[+14]	4.58[+13]
4*B*	$(1s2s4p_{1/2})_{1/2}\rightarrow 1s^24s$	2.3936	⟨2.394⟩	4796.3	1.68[+13]	1.18[+13]	1.19[+13]
4*B*	$(1s2p_{1/2}4p_{3/2})_{3/2}\rightarrow 1s^24p_{3/2}$	2.3947	⟨2.394⟩	4799.8	8.44[+12]	1.29[+13]	9.65[+12]
4*B*	$(1s2p_{1/2}4d_{5/2})_{7/2}\rightarrow 1s^24d_{5/2}$	2.3948	⟨2.394⟩	4801.8	5.95[+11]	1.18[+13]	4.53[+12]
4*B*	$(1s2p_{1/2}4p_{3/2})_{5/2}\rightarrow 1s^24p_{3/2}$	2.3958	⟨2.394⟩	4799.9	2.50[+12]	1.44[+13]	1.25[+13]
4*C*	$(1s2s4p_{3/2})_{3/2}\rightarrow 1s^24d_{5/2}$	2.3972	⟨2.398⟩	4797.0	5.93[+12]	2.99[+12]	4.12[+12]
4*C*	$(1s2s4s)_{1/2}\rightarrow 1s^24p_{3/2}$	2.3987	⟨2.398⟩	4791.1	8.38[+12]	5.02[+12]	4.98[+12]
			$n=5$				
5*A*	$(1s2p_{3/2}5d_{5/2})_{5/2}\rightarrow 1s^25d_{3/2}$	2.3826	⟨2.3824⟩	4963.3	2.91[+12]	1.12[+14]	7.26[+12]
5*A*	$(1s2p_{3/2}5d_{5/2})_{5/2}\rightarrow 1s^25d_{5/2}$	2.3827	⟨2.3824⟩	4963.3	2.91[+12]	1.55[+14]	1.00[+13]
5*A*	$(1s2p_{3/2}5d_{3/2})_{5/2}\rightarrow 1s^25d_{3/2}$	2.3828	⟨2.3824⟩	4963.0	1.18[+12]	1.56[+14]	4.04[+12]
5*A*	$(1s2p_{3/2}5p_{3/2})_{1/2}\rightarrow 1s^25p_{3/2}$	2.3829	⟨2.3824⟩	4962.0	2.65[+12]	2.31[+14]	4.45[+12]
5*A*	$(1s2p_{3/2}5d_{5/2})_{7/2}\rightarrow 1s^25d_{5/2}$	2.3829	⟨2.3824⟩	4962.9	3.44[+12]	2.72[+14]	2.71[+13]
5*A*	$(1s2p_{3/2}5p_{3/2})_{3/2}\rightarrow 1s^25p_{3/2}$	2.3831	⟨2.3824⟩	4961.4	1.54[+12]	2.68[+14]	6.02[+12]
5*A*	$(1s2p_{3/2}5p_{1/2})_{3/2}\rightarrow 1s^25p_{1/2}$	2.3831	⟨2.3824⟩	4960.7	5.67[+12]	2.68[+14]	2.19[+13]
5*A*	$(1s2p_{3/2}5p_{3/2})_{5/2}\rightarrow 1s^25p_{3/2}$	2.3832	⟨2.3824⟩	4961.1	3.78[+12]	2.71[+14]	2.19[+13]
5*B*	$(1s2s5p_{1/2})_{1/2}\rightarrow 1s^25s$	2.3937	⟨2.394⟩	4935.2	7.77[+12]	4.97[+12]	4.69[+12]
5*B*	$(1s2p_{1/2}5p_{3/2})_{1/2}\rightarrow 1s^25p_{3/2}$	2.3943	⟨2.394⟩	4936.9	4.57[+12]	1.36[+13]	8.32[+12]
5*B*	$(1s2p_{1/2}5p_{3/2})_{5/2}\rightarrow 1s^25p_{3/2}$	2.3948	⟨2.394⟩	4935.9	1.72[+13]	1.38[+13]	9.02[+12]
			$n=6$				
6*A*	$(1s2p_{3/2}6d_{5/2})_{5/2}\rightarrow 1s^26d_{5/2}$	2.3826	⟨2.3824⟩	5037.1	1.63[+12]	1.66[+14]	6.01[+12]
6*A*	$(1s2p_{3/2}6d_{5/2})_{7/2}\rightarrow 1s^26d_{5/2}$	2.3826	⟨2.3824⟩	5036.8	2.01[+12]	2.72[+14]	1.60[+13]
6*A*	$(1s2p_{3/2}6p_{1/2})_{3/2}\rightarrow 1s^26p_{1/2}$	2.3828	⟨2.3824⟩	5035.6	3.20[+12]	2.69[+14]	1.25[+13]
6*A*	$(1s2p_{3/2}6p_{3/2})_{5/2}\rightarrow 1s^26p_{3/2}$	2.3828	⟨2.3824⟩	5035.6	2.12[+12]	2.71[+14]	1.24[+13]
6*B*	$(1s2p_{1/2}6p_{3/2})_{3/2}\rightarrow 1s^26p_{3/2}$	2.3942	⟨2.3933⟩	5011.2	2.54[+12]	1.39[+13]	6.10[+12]
6*B*	$(1s2p_{1/2}6p_{3/2})_{5/2}\rightarrow 1s^26p_{3/2}$	2.3944	⟨2.3933⟩	5010.7	1.08[+12]	1.48[+13]	5.94[+12]

TABLE VIII. Atomic data for the principal dielectronic satellite transitions $1s^2 2lnl'$-$1s2l^2nl'$ ($n=4,5,6$) in berylliumlike V^{19+}. Only transitions with line factor $F_2 > 3.5\times10^{12}$ s^{-1} are listed. Experimental wavelengths are measured with respect to the heliumlike reference line w set to the semiempirical value of 2.381 87 Å. ⟨ ⟩ denotes blends. $a[b]=a\times10^b$.

Key	Transition	λ_{theor} (Å)	λ_{expt} (Å)	E_{au} (eV)	A_a^{si} (s^{-1})	$\sum_j A_a^{sj}$ (s^{-1})	A_r^{sf} (s^{-1})	f_2 (s^{-1})
				$n=4$				
4C	$(1s2s2p_{3/2}4d_{3/2})_3 \rightarrow (1s^2 2s4d_{5/2})_2$	2.3986	⟨2.398⟩	4827.9	5.81[+12]	7.57[+13]	2.12[+14]	9.27[+12]
4C	$(1s2s2p_{3/2}4p_{3/2})_0 \rightarrow (1s^2 2s4p_{3/2})_1$	2.3987	⟨2.398⟩	4821.8	5.23[+12]	1.30[+13]	2.55[+14]	9.76[+12]
4C	$(1s2s2p_{3/2}4d_{5/2})_4 \rightarrow (1s^2 2s4d_{5/2})_3$	2.3987	⟨2.398⟩	4825.6	5.25[+12]	2.24[+13]	2.58[+14]	1.01[+13]
4C	$(1s2s2p_{3/2}4p_{3/2})_2 \rightarrow (1s^2 2s4p_{3/2})_2$	2.3991	⟨2.398⟩	4820.4	5.78[+12]	1.69[+14]	1.10[+14]	4.65[+12]
4C	$(1s2s2p_{3/2}4p_{1/2})_2 \rightarrow (1s^2 2s4p_{1/2})_1$	2.3993	⟨2.398⟩	4819.2	7.42[+12]	1.64[+14]	2.30[+14]	1.25[+13]
4C	$(1s2s2p_{3/2}4p_{3/2})_2 \rightarrow (1s^2 2s4p_{3/2})_1$	2.3993	⟨2.398⟩	4820.4	5.78[+12]	1.69[+14]	1.45[+14]	6.14[+12]
4C	$(1s2s2p_{3/2}4p_{3/2})_3 \rightarrow (1s^2 2s4p_{3/2})_2$	2.3995	⟨2.398⟩	4819.6	6.20[+12]	1.17[+13]	2.52[+14]	1.14[+13]
				$n=5$				
5C	$(1s2s2p_{3/2}5d_{5/2})_4 \rightarrow (1s^2 2s5d_{5/2})_3$	2.3982	⟨2.398⟩	4950.7	2.81[+12]	1.23[+13]	2.60[+14]	5.51[+12]
5C	$(1s2s2p_{3/2}5p_{3/2})_0 \rightarrow (1s^2 2s5p_{3/2})_1$	2.3983	⟨2.398⟩	4948.5	2.72[+12]	7.51[+12]	2.48[+14]	5.12[+12]
5C	$(1s2s2p_{3/2}5d_{3/2})_3 \rightarrow (1s^2 2s5d_{5/2})_2$	2.3983	⟨2.398⟩	4951.6	3.08[+12]	9.95[+13]	1.89[+14]	4.44[+12]
5C	$(1s2s2p_{3/2}5p_{3/2})_3 \rightarrow (1s^2 2s5p_{3/2})_2$	2.3986	⟨2.398⟩	4947.6	3.09[+12]	4.88[+13]	2.51[+14]	5.85[+12]
5C	$(1s2s2p_{3/2}5p_{1/2})_2 \rightarrow (1s^2 2s5p_{1/2})_1$	2.3986	⟨2.398⟩	4947.3	3.56[+12]	1.57[+14]	2.33[+14]	5.95[+12]
				$n=6$				
6C	$(1s2s2p_{3/2}6p_{1/2})_2 \rightarrow (1s^2 2s6p_{1/2})_1$	2.3983	⟨2.397⟩	5016.2	2.00[+12]	1.54[+14]	2.41[+14]	3.71[+12]

strong high-n heliumlike satellite lines are found only close to w and y. By contrast, all lithiumlike lines that are formed by innershell excitation from the ground state are dipole allowed and have radiative rates larger than 10^{12} s^{-1} (cf. Table II). Therefore high-n lithiumlike satellite lines are predicted to be located near lithiumlike lines q through v; the strongest, however, are located near the position of q, as q has the largest radiative rate. These results are summarized in Table VII, where we list the strongest high-n dielectronic satellites lines from lithiumlike ions, and in Table VIII, which lists the strongest high-n dielectronic satellites from berylliumlike ions.

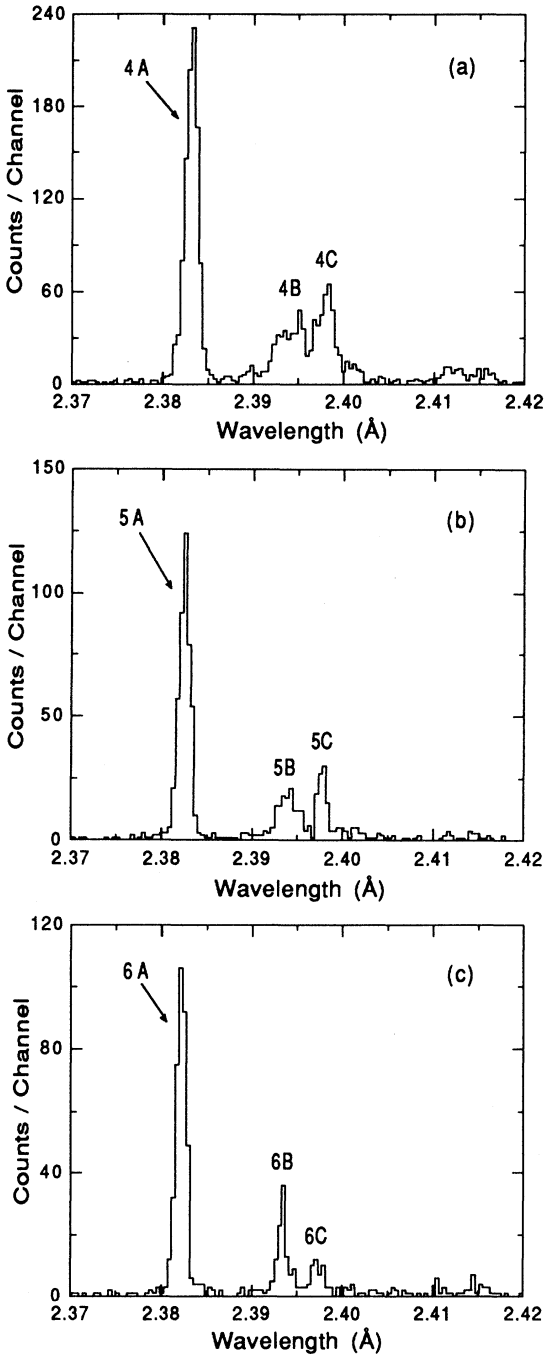

FIG. 4. High-n satellite spectra of V^{21+}. The beam energy was set to (a) the *KLN* resonance at 4780 eV, (b) the *KLO* resonance at 4930 eV, and (c) the *KLP* resonance at 5020 eV. The features labeled A and B consist of satellite lines from lithiumlike ions; C consists predominantly of satellite lines from berylliumlike ions.

Our expectations are confirmed by the spectra shown in Figs. 4(a)–4(c). These are obtained at beam energies of 4780, 4930, and 5020 eV corresponding to the energies of the *KLN*, *KLO*, and *KLP* resonances, respectively. Each spectrum shows three distinct features labeled A, B, and C. Features A and B are satellite lines from lithiumlike ions, which form on the low-energy side of their heliumlike parent lines w and y. Feature C is largely due to satellite lines from berylliumlike ions near their lithiumlike parent line q. Because of their low intensity, no high-n satellites located near lithiumlike parent lines r through v have been identified.

The interaction between the spectator and core electrons decreases, as n increases. As a result, the transition energies of high-n dielectronic satellites approaches that of their respective parent lines. This manifests itself in Fig. 4 in two ways. First, the widths of features A, B, and C narrow as n increases; second, their central position approaches that of their parent lines. The spectra in Fig. 4 can also be compared to Fig. 3, where features $3A$, $3B$, and $3C$ are much broader and extend over a large wavelength range. Very high-n satellite transitions have recently been studied for heliumlike Ti^{20+} [39]. Such transitions are virtually indistinguishable from their dipole-allowed parent lines.

Average wavelengths have been determined for the features in Fig. 4 and are given in Tables VII and VIII. The measured values are found to be somewhat lower than calculated.

VIII. NOTE ON SATELLITE INTENSITIES

The present measurements do not allow us to determine the dielectronic recombination cross sections. Nevertheless, we can make some statements about the relative satellite intensities.

We have modeled the observed spectra using the atomic data in Tables II–VIII. A typical model spectrum for a beam energy of 3700 eV and assuming a spread in electron energy of 100 eV is shown in Fig. 5. The model calculations do not account for the fact that line emission from EBIT is generally polarized because of alignment arising from interactions with the electron beam [40]. Since crystal spectrometers act as polarizers, lines are diffracted differently depending on their polarization. Line intensities are also affected by angular anisotropies of the x-ray emission, again depending on their polarization. Although polarization effects are not accounted for, a comparison of the model spectrum with the data in Fig. 2(b) shows good overall agreement. Definite discrepancies are only found for the relative intensities of the satellite lines from berylliumlike ions. These may in part be due to inaccuracies in the theoretical wavelengths.

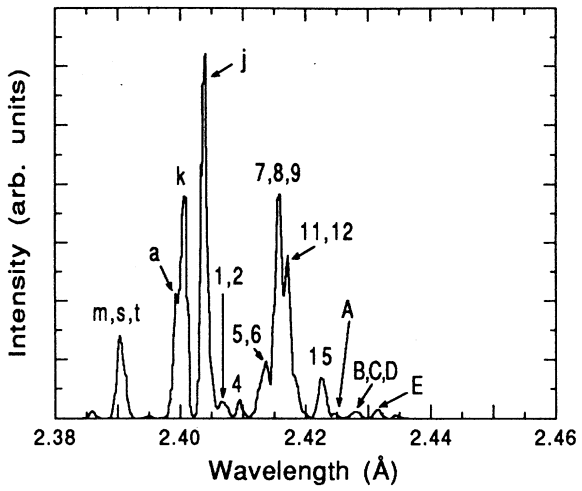

FIG. 5. Theoretical spectrum of the dielectronic satellite transitions at a beam energy of 3700 eV and a beam energy spread of 100-eV FWHM. Spectral linewidths with $\lambda/\Delta\lambda=2700$ are assumed to allow summing of adjoining transitions and comparison with the experimental spectrum in Fig. 2(b). The assumed charge balance is He:Li:Be=1:0.75:0.15. The calculations do not include polarization or angular distribution of the line emission.

The satellite transitions *o* and *p* share the same upper level $1s2s^2$ (cf. Table II) and are the result of the same dielectronic resonance. The ratio of their intensities, therefore, is given by the ratio of their radiative rates. Lines *o* and *p* are well resolved, yet sufficiently close so that we do not have to be concerned with differential detector efficiency. Moreover, *o* and *p* are unpolarized, because their mutual upper level has a total angular momentum $J=\frac{1}{2}$. As a result, their ratio can be determined directly from our spectral observations without further corrections, and error limits are determined by statistics. The result is given in Table IX. The measured ratio is somewhat smaller than predicted, but the difference is not statistically significant.

TABLE IX. Comparison of measured intensity ratio of satellites *p* to *o* with theoretical predictions.

Experiment	Theory[a]	Theory[b]
0.72±0.13	0.81	0.84

[a]Present MCDF calculations.
[b]Vainshtein and Safronova, Ref. [31].

IX. CONCLUSION

High-resolution crystal measurements of the dielectronic satellite spectrum of heliumlike vanadium were presented that were obtained in interactions of vanadium ions with an electron beam. We were able to selectively excite and observe dielectronic resonances and to identify many transitions for the first time in an x-ray spectrum.

The present investigation suggests the possibility of measuring the resonance strength of individual satellite lines by making use of the resolving power of crystal spectrometers. For such a measurement the electron-beam energy must be alternated or swept across the resonances in such a way as to keep the ionization balance unchanged similar to the procedure used in the measurement of the total *KLL* resonance strength of heliumlike nickel by Knapp *et al.* [12]. Although this drastically reduces the duty cycle, exploratory measurements of heliumlike iron have shown that such a measurement is feasible [41] so that level-specific dielectronic recombination cross-section measurements should be possible in the near future.

ACKNOWLEDGMENTS

We thank E. Magee and D. Nelson for their expert technical support. We are indebted to Dr. E. Källne from the Royal Institute of Technology of Sweden for lending us the detector used in the measurements. This work was performed under the auspices of the U.S. Department of Energy by Lawrence Livermore National Laboratory under Contract No. W-7405-ENG-48.

[1] A. H. Gabriel, Mon. Not. R. Astron. Soc. **160**, 99 (1972).
[2] J. Dubau and S. Volonté, Rep. Prog. Phys. **43**, 199 (1980).
[3] M. Bitter, K. W. Hill, N. R. Sauthoff, P. C. Efthimion, E. Merservey, W. Roney, S. von Goeler, R. Horton, M. Goldman, and W. Stodiek, Phys. Rev. Lett. **43**, 129 (1979).
[4] S. von Goeler, M. Bitter, S. Cohen, D. Eames, K. W. Hill, D. Hills, R. Hulse, G. Lenner, D. Manos, P. Roney, N. Sauthoff, S. Sesnic, W. Stodiek, F. Tenney, and J. Timberlake, in *Proceedings of the Course on Diagnostics for Fusion Reactor Conditions, Varenna, 1982,* edited by P. E. Stott *et al.* (Commission of the European Communities, Brussels, 1983), Vol. I, p. 109.
[5] M. L. Apicella, R. Bartiromo, F. Bombarda, and R. Giannella, Phys. Lett. **98A**, 174 (1983).
[6] R. Bartiromo, F. Bombarda, and R. Giannella, Phys. Rev. A **32**, 531 (1985).
[7] J. F. Seely, U. Feldman, and G. A. Doschek, Astrophys. J. **319**, 541 (1987).
[8] E. Källne and J. Källne, Phys. Scr. **T17**, 152 (1987).
[9] G. A. Doschek, in *X-ray and Inner-Shell Processes, Knoxville, 1990,* Proceedings of the Conference on X-ray and Inner Shell Processes, edited by T. A. Carlson, M. O. Krause, and S. T. Manson, AIP Conf. Proc. No. 215 (AIP,

New York, 1990), p. 603.
[10] R. E. Marrs, M. A. Levine, D. A. Knapp, and J. R. Henderson, Phys. Rev. Lett. **60**, 1715 (1988).
[11] M. A. Levine, R. E. Marrs, J. R. Henderson, D. A. Knapp, and M. B. Schneider, Phys. Scr. **T22**, 157 (1988).
[12] D. A. Knapp, R. E. Marrs, M. A. Levine, C. L. Bennett, M. H. Chen, J. R. Henderson, M. B. Schneider, and J. H. Scofield, Phys. Rev. Lett. **62**, 2104 (1989).
[13] R. Ali, C. P. Bhalla, C. L. Cocke, and M. Stöckli, Phys. Rev. Lett. **64**, 633 (1990).
[14] L. H. Andersen, P. Hvelplund, H. Knudsen, and P. Kvistgaard, Phys. Rev. Lett. **62**, 2656 (1989).
[15] S. Datz, C. R. Vane, P. F. Dittner, J. P. Giese, J. Gomez del Campo, N. L. Jones, H. F. Krause, P. D. Miller, M. Schulz, H. Schöne, and T. M. Rosseel, Phys. Rev. Lett. **63**, 742 (1989).
[16] I. P. Grant, B. J. McKenzie, P. H. Norrington, D. F. Mayers, and N. C. Pyper, Comput. Phys. Commun. **21**, 207 (1980).
[17] M. H. Chen, Phys. Rev. A **31**, 1449 (1985).
[18] M. H. Chen, At. Data Nucl. Data Tables **34**, 301 (1986).
[19] P. Beiersdorfer, R. E. Marrs, J. R. Henderson, D. A. Knapp, M. A. Levine, D. B. Platt, M. B. Schneider, D. A. Vogel, and K. L. Wong, Rev. Sci. Instrum. **61**, 2338 (1990).
[20] W. R. Johnson and G. Soff, At. Data Nucl. Data Tables **33**, 405 (1985).
[21] G. W. F. Drake, Can. J. Phys. **66**, 586 (1988).
[22] L. A. Vainshtein and U. I. Safronova, Phys. Scr. **31**, 519 (1985).
[23] P. Beiersdorfer, M. Bitter, S. von Goeler, and K. W. Hill, Phys. Rev. A **40**, 150 (1989).
[24] P. J. Mohr, in *Beam-Foil Spectroscopy,* edited by I. A. Sellin and D. J. Pegg (Plenum, New York, 1976), Vol. I, p. 97.
[25] H. L. Zhang and D. H. Sampson (private communication).
[26] TFR Group, M. Cornille, J. Dubau, and M. Loulergue, Phys. Rev. A **32**, 3000 (1985).
[27] M. Bitter, K. W. Hill, M. Zarnstorff, S. von Goeler, R. Hulse, L. C. Johnson, N. R. Sauthoff, S. Sesnic, and K. M. Young, Phys. Rev. A **32**, 3011 (1985).
[28] J. F. Seely, U. Feldman, and U. I. Safronova, Astrophys. J **304**, 838 (1986).
[29] P. Beiersdorfer, T. W. Phillips, V. L. Jacobs, K. W. Hill, M. Bitter, S. von Goeler, and S. Kahn (unpublished).
[30] M. Bitter, H. Hsuan, J. E. Rice, K. W. Hill, M. Diesso, B. Grek, R. Hulse, D. W. Johnson, L. C. Johnson, and S. von Goeler, Rev. Sci. Instrum. **59**, 2131 (1988).
[31] L. A. Vainshtein and U. I. Safronova, At. Data Tables **25**, 49 (1978).
[32] F. Bely-Dubau, A. H. Gabriel, and S. Volonté, Mon. Not. R. Astron. Soc. **186**, 405 (1979).
[33] F. Bely-Dubau, A. H. Gabriel, and S. Volonté, Mon. Not. R. Astron. Soc. **189**, 801 (1979).
[34] M. Bitter, S. von Goeler, K. W. Hill, R. Horton, D. Johnson, W. Roney, N. Sauthoff, E. Silver, and W. Stodiek, Phys. Rev. Lett. **47**, 921 (1981).
[35] F. Bely-Dubau, P. Faucher, L. Steenman-Clark, M. Bitter, S. von Goeler, K. W. Hill, C. Cmahy-Val, and J. Dubau, Phys. Rev. A **26**, 3459 (1982).
[36] K.-D. Zastrow, E. Källne, and H. P. Summers, Phys. Rev. A **41**, 1427 (1990).
[37] R. D. Cowan, *The Theory of Atomic Structure and Spectra* (University of California Press, Berkeley, 1981), p. 557.
[38] C. D. Lin, W. R. Johnson, and A. Dalgarno, Phys. Rev. A **15**, 154 (1977).
[39] P. Beiersdorfer, S. Chantrenne, M. H. Chen, R. Marrs, D. Vogel, K. Wong, and R. Zasadzinski, Z. Phys. D (to be published).
[40] J. R. Henderson, P. Beiersdorfer, C. L. Bennett, S. Chantrenne, D. A. Knapp, R. E. Marrs, M. B. Schneider, K. L. Wong, G. A. Doschek, J. F. Seely, C. M. Brown, R. E. LaVilla, J. Dubau, and M. A. Levine, Phys. Rev. Lett. **65**, 705 (1990).
[41] P. Beiersdorfer, Nucl. Instrum. Methods B (to be published).